Quantum oscillations in the mixed state of the type II superconductor 2H-NbSe$_2$

Quantum oscillations in the mixed state of the type II superconductor 2H-NbSe$_2$

R Corcoran†, P Meeson†, Y Onuki‡, P-A Probst†, M Springford†, K Takita‡, H Harima†||, G Y Guo§ and B L Gyorffy†

† H H Wills Physics Laboratory, University of Bristol, Royal Fort, Tyndall Avenue, Bristol BS8 1TL, UK
‡ Institute of Material Science, University of Tsukuba, Tsukuba, Ibaraki 305, Japan
§ SERC Daresbury Laboratory, Warrington WA4 4AD, UK

Abstract. Quantum oscillations have been investigated far into the mixed state of the type II superconductor 2H-NbSe$_2$. The de Haas–van Alphen effect is found to persist to fields as low as $\sim 0.3B_{C2}$ and to temperatures of $\sim 0.003T_C$. A self-consistent band structure calculation, performed for 2H-NbSe$_2$ in the normal non-charge-density-wave state using a full potential linearized augmented plane wave (FLAPW) method, accounts well for the experimental angular dependence of the quantum oscillations in terms of a small flat hole Fermi surface around the Γ point. This feature derives mainly from chalcogen p bands and has a mass-enhancement factor much smaller than expected from the specific heat. Quantum oscillations in the presence of the vortex lattice are observed to experience an additional damping, from which the order parameter is estimated to be $\Delta(0) = 0.6 \pm 0.1$ meV.

1. Introduction

The existence of quantum oscillations in a system at low temperatures and high magnetic fields is normally regarded as an unambiguous signature of the existence of a Fermi surface. Much interest therefore is attached to the possibility of performing such measurements in a high-temperature superconductor as a means of probing the normal state in these intriguing materials. However, since the values of B_{C2} in them are mostly considerably in excess of the magnetic fields attainable in the laboratory, it is necessary to consider the possibility of observing quantum oscillations in the vortex state of these strongly type II materials.

In fact quantum oscillations in the form of magnetothermal [1] and de Haas–van Alphen (DHVA) effect oscillations [2] have already been observed in the mixed state in the dichalcogenide layered superconductor 2H-NbSe$_2$. More recently, such oscillations have also been reported YBCO [3–6], V$_3$Si [7,8], Nb$_3$Sn [9], Ba(K)BiO$_3$ [10] and the organic superconductor κ-(ET)$_2$Cu(NCS)$_2$ [11]. The existence of such oscillations within the magnetically inhomogeneous environment of the vortex state is surprising enough, but what is more so is that they should persist down to low temperatures ($T/T_C \ll 1$) and low magnetic fields ($B/B_{C2} < 1$). Under these conditions the number of electrons contributing to the superconducting state, proportional to $|\Delta|^2$ (Δ being the superconducting order parameter), is nearly saturated. Assuming that this quantum oscillatory phenomenon is

|| Permanent address: College of Integrated Arts and Sciences, University of Osaka Prefecture, Sakai, Osaka 593, Japan.

due to the conventional mechanism of fermions in Landau orbits it is pertinent to inquire where such quasiparticles may come from under the above circumstances. The confinement of the normal electrons to the vortex core does not seem to allow the semi-classical picture of electrons in quantized cyclotron orbits to be applied, as the radius of the would-be cyclotron orbit, r_c, in the fields used is much larger than the coherence length ξ (e.g. in NbSe$_2$ at $B = 8$ T, $r_c = 560$ Å and $\xi = 30$ Å at $T = 40$ mK). To account for their results in 2H-NbSe$_2$, Onuki *et al* [2] postulated a novel state of matter in which normal and superconducting sheets of the Fermi surface co-exist.

Several theories have been advanced to explain the origin of quantum oscillations in the mixed state. Most of these [12–16] conclude that an additional exponential damping term arises as the order parameter develops at and below B_{C2}, although the mechanism for this varies amongst the different authors. For a 2D electron gas, Maniv *et al* [17] have considered the pairing of electrons already in Landau levels and found oscillations of both the superconducting order parameter and the free energy of the superconducting electrons. Their scheme would lead to quantum oscillations of the magnetization in the superconducting regime having a different character to those in the normal state, and possibly also leading to re-entrant superconductivity at sufficiently large fields [18].

It was against this background that the present work was undertaken, to clarify the physics underlying the existence of quantum oscillations in the mixed state of a superconductor. New experiments have been performed in 2H-NbSe$_2$ of greater accuracy and over a substantially greater range of magnetic field and temperature than those employed previously. A self-consistent band structure calculation has also been carried out for the normal non-CDW state of 2H-NbSe$_2$ using the FLAPW method. Previous calculations [19–21] were not self-consistent and shape approximations were made to the potentials. The present calculation explains, for the first time, the Fermi surface feature observed in DHVA effect experiments in the normal state of 2H-NbSe$_2$. Quantum oscillations are observed to persist into the superconducting state to fields as low as $\sim 0.3 B_{C2}$ and to temperatures of $\sim 0.003 T_C$, although with an additional damping when compared to the normal state. We argue that the origin of quantum oscillations under these conditions may be traced to the intrinsic gaplessness of strongly type II, inhomogeneous superconductors for quasiparticle excitations with k-vectors normal to the applied field [22]: i.e. precisely those probed in such experiments. In fact the theories of Maki [12] and of Wasserman and Springford [13] predict an additional damping of the de Haas–van Alphen amplitude in the superconducting state determined by the square of the orbitally averaged order parameter. We interpret our results in terms of these theories.

2. Experimental details

A stack of four crystals was used for these experiments each measuring $\sim 1.5 \times 5 \times 0.2$ mm^3 (the short direction being the c-axis of the hexagonal crystal structure). The crystals were grown by iodine vapour transport and their structure and composition were analysed using x-rays and XPS. They were confirmed to have the structure 2H-NbSe$_2$ and to be single phase. Resistivity measurements, shown in figure 1, yielded a resistivity ratio, $\rho_{300 \text{ K}}/\rho_0$, of 50 and showed in their temperature dependence a feature at $T_D = 33$ K attributed to the CDW instability which is known to exist in this material. The superconducting transition temperature, T_C, of the samples was found to be 7.2 K. Both T_C and T_D agree well with expected previously measured values for these transitions [23].

DHVA measurements were made in a top-loading mixing (TLM) chamber dilution refrigerator over the temperature range 20 mK–4.2 K in magnetic fields up to 13.6 T.
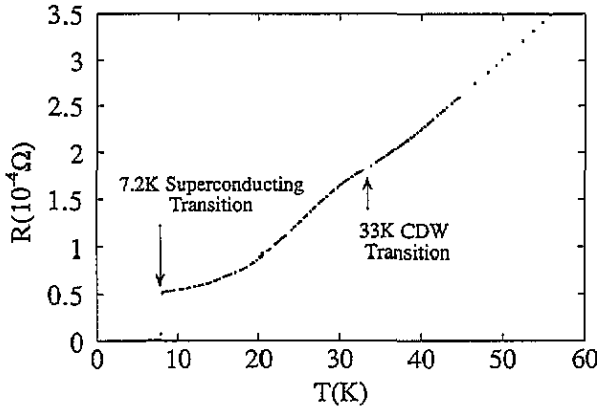
Figure 1. Resistance measurements of a 2H-NbSe$_2$ single crystal. The onset of the charge density wave is seen as an increase in the resistivity at $T_D \approx 33$ K. The superconducting transition is at $T_C = 7.2$ K.

A superconducting modulation coil situated in the main magnet was used to make AC susceptibility measurements using the field modulation technique [24]. The magnetization of the samples was measured using a pair of side-by-side compensated coils with square cross section, balanced to 0.05%. For most of the experiments a modulation field of 0.03 T at 5.2 Hz was used to minimize sample heating effects

NbSe$_2$ is an anisotropic superconductor ($\kappa_\parallel \approx 54$ and $\kappa_\perp \approx 14$, parallel and perpendicular to the planes respectively, where $\kappa = \lambda/\xi$), the upper critical field, B_{C2}, depends on the orientation relative to the magnetic field direction. In most experiments the c-axis was aligned 70° from the field direction to give $B_{C2} = 9.3$ T at 20 mK. This allowed quantum oscillations to be observed over a considerable range of fields both above and below B_{C2}.

3. DHVA amplitude and analysis

According to the semiclassical theory of Lifshitz and Kosevich (LK) for the DHVA effect in a normal metal measured using the field modulation technique, the amplitude of the voltage induced in a pick-up coil coupled to the sample is [24]

$$V_r = \frac{2.6093\omega\phi G J_2(\lambda) T B^{-1/2} F R_T R_D S_r}{r^{1/2}|A''|^{1/2}X} \tag{1}$$

in which r refers to the harmonic of the DHVA effect, ω is the modulation frequency, ϕ is the coupling to the detection coil, G the gain, F is the DHVA frequency and $J_2(\lambda)$ a second-order Bessel function with argument $\lambda = 2\pi r b_0 F/B^2$ where b_0 is the peak amplitude of the modulation field $b = b_0 \sin \omega t$. In these experiments the phase sensitive detection was at $2f_m$, the angular modulation frequency being $\omega = 2\pi f_m$. $S_r = \cos(\pi r g m/2m_e)$ is the spin factor which accounts for the effect of Zeeman splitting of the Landau levels. R_T is a damping term due to thermal broadening of the Landau levels, whose form follows from the Fermi–Dirac distribution function

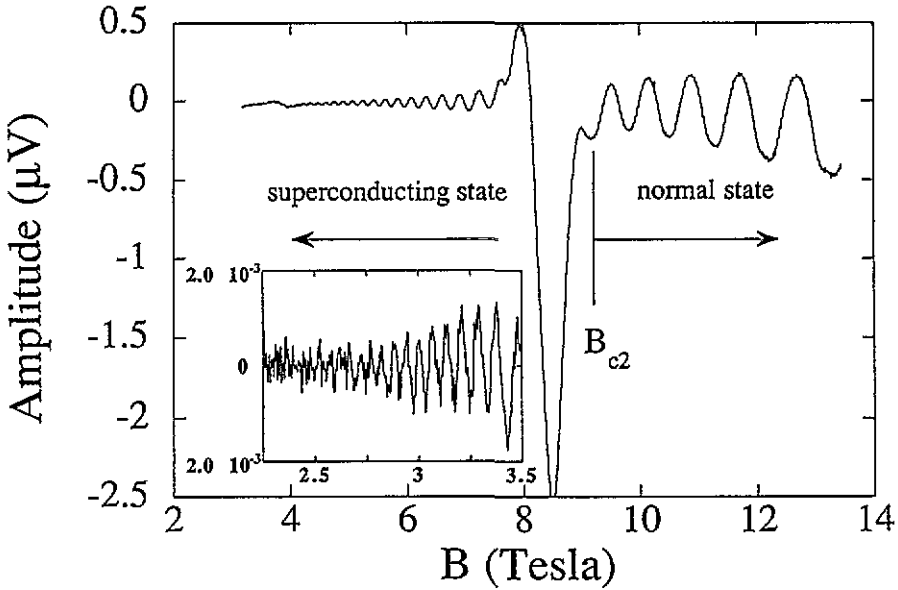$$R_T = \frac{X}{\sinh(X)} \qquad \text{where } X = \frac{-Krm^*T}{B}. \tag{2}$$

Figure 2. DHVA effect in 2H-NbSe₂ at 24 mK with the field inclined at 70° to the *c*-axis. The inset shows oscillations persisting to fields ≈ 2.5 T.

$K = 2\pi^2 k_B m_e/e\hbar = 14.69$. By fitting the measured temperature dependence of the DHVA amplitude at fixed magnetic field to this expression, the effective mass m^* is determined. The damping of the DHVA signal caused by scattering due to defects and impurities is described by the term R_D,

$$R_D = \exp\left\{\frac{-\pi}{\omega_c \tau_0}\right\} \tag{3}$$

where τ_0 is the electron scattering lifetime and ω_c is the cyclotron frequency eB/m^*.

The measured DHVA amplitude, A_{SC}, in the superconducting state can be compared to the DHVA amplitude, A_N, expected from the LK theory. Parameters obtained from the data above B_{C2}, in the normal state, can be used to calculate A_N. The attenuation in the mixed state can be displayed by plotting the ratio A_{SC}/A_N versus $1/B$. In each case the temperature dependence, experimental gains and $1/\sqrt{B}$ field dependence are taken out of the amplitudes such that

$$A_{N/SC} = V_r \frac{r^{1/2} B^{1/2} \sinh(Krm^*T/B)}{G J_2(\lambda) T}. \tag{4}$$

4. Experimental results

A typical record of the DHVA effect at 20 mK with the *c*-axis at 70° to the *B* field is shown in figure 2. The transition to the vortex state is signalled by the large feature that starts at 9.3 T and has a width ≈ 1.5 T. It shows hysteresis upon reversing the direction of the field sweep suggesting that flux pinning probably plays a role. DVHA oscillations of frequency $F = 152 \pm 1$ T can clearly be seen above and below B_{C2}, extending to fields as low as 2.5 T, the phase and frequency remaining unchanged.

Rotation of the crystal with respect to the magnetic field yielded a frequency variation in good agreement with that reported previously [1, 2]. The DHVA frequency

$$F = \hbar S / 2\pi e \tag{5}$$

may be fitted well to the form of an oblate spheroid where S is given by

$$S = \frac{\pi k_a^2}{(\sin^2 \theta + (k_a/k_c)^2 \cos^2 \theta)} \tag{6}$$

where the major and minor axes, $2k_a$ and $2k_c$, are 0.338 ± 0.006 Å^{-1} and 0.050 ± 0.002 Å^{-1} respectively. Such a variation is characteristic of a small ellipsoidal sheet of Fermi surface occupying only 0.03% of the Brillouin zone. No other orbits were observed in these experiments, even with the c-axis aligned parallel to the applied field.

DHVA oscillations were studied over the temperature range 0.02–4.2 K in the normal state, and 0.02–2 K in the superconducting state. In each case, as shown in figure 3, the temperature dependence at a constant field could be fitted reasonably well to equation (2). From these fits values of m^* for the observed orbit in the normal and superconducting state were determined as $(0.62 \pm 0.005)m_e$ $(B = 11.1$ T$)$ and $(0.6 \pm 0.01)m_e$ $(B = 5.3$ T$)$ respectively, in close agreement with each other. Amplitude analysis in the normal state reveals that the crystals used had an electron scattering rate $1/\tau_0 = 2.1 \times 10^{-12}$ s^{-1} (or equivalently a Dingle temperature of 2.5 K). The amplitude plot in figure 4, however, revealed that there is a small additional damping, $R_S = A_{SC}/A_N$, of the DHVA signal on passing from the normal to the superconducting state.
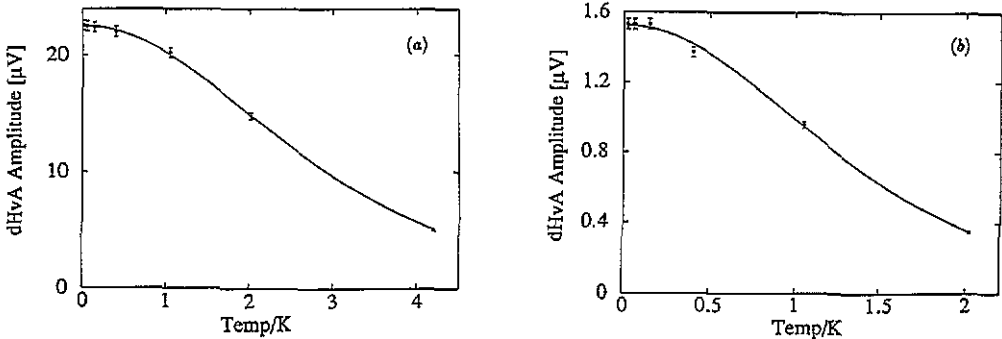

Figure 3. The temperature dependence of the DHVA effect in 2H-NbSe$_2$ in the (a) normal $(B = 11.1$ T$)$ and (b) mixed state $(B = 5.3$ T$)$. The solid lines are the best fits to the variation expressed in equation (2).

As mentioned above, the nature and origin of quantum oscillations originating from the mixed state of a superconductor has not yet been clearly resolved. We note, however, that similar experimental observations to those reported here were also made by Corcoran *et al* [8] in V$_3$Si. There too DHVA oscillations suffered an additional damping in the mixed state whose magnitude and field dependence could be accounted for reasonably well according to the theories of Maki [12] and Wasserman and Springford [13]. These approaches make use of the vortex state self-energy obtained by Brandt *et al* [22] who considered approximations valid close to B_{C2}. An important feature of this self-energy is
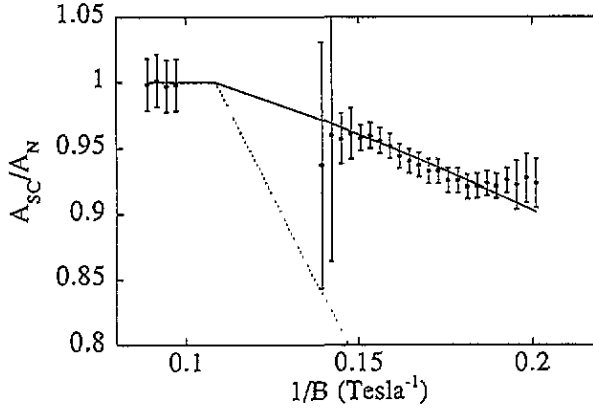
Figure 4. Damping of the DVHA signal in the mixed state relative to the normal state (A_{SC}/A_N). The solid and dotted lines illustrate the amplitude reduction calculated according to theory [12, 13] with values $\Delta(0) = 0.6$ meV and 1.1 meV respectively.

its anisotropy which leads to BCS-like behaviour for excitations with wavevector parallel to B, but to a *gapless* state for perpendicular wavevectors. While in a simple model, the real part of the self-energy vanishes, leading to an unchanged DHVA frequency, the finite imaginary part leads to damping which we write as

$$R_s = \exp\left(\frac{-\pi}{\omega_c \tau_s}\right) \qquad (7)$$

where τ_s is a field-dependent scattering rate,

$$\tau_s^{-1} = \frac{2\pi^{1/2}\Delta^2 \Lambda}{\hbar v_F}. \qquad (8)$$

Here Δ is the orbitally averaged order parameter, $\Lambda = (2\hbar e B)^{-1/2}$ and v_F is the orbitally averaged Fermi velocity. If we further assume, as in [12], that the field dependence of Δ varies according to

$$\Delta^2 = \Delta^2(0)(1 - B/B_{C2}) \qquad (9)$$

the damping R_s can be calculated for direct comparison with the experimental data. The result of this is shown by the dotted line in figure 4, for which the value $\Delta(0) = 1.1$ meV was assumed, as determined from infra-red and Raman experiments [25, 26]. As is clearly seen, however, this is a poor representation of the experiments which are in agreement with the substantially smaller value (solid line) of $\Delta(0) = 0.6$ meV. We shall return to this after first presenting the band structure.

5. Band structure calculation

A self-consistent band structure calculation has been carried out using a FLAPW method, and the Gunnarson and Lundqvist formula [27] for the exchange–correlation potential. The crystal structure of 2H-NbSe$_2$ is shown in figure 5 and the parameters used in the calculation

Table 1. Crystal structure and parameters used in the calculation for 2H-NbSe$_2$.

Space group	No 194 D$_{6h}^4$
Lattice constant	$a = 3.45$ Å, $c = 12.54$ Å
Atomic positions	
Nb	$(0, 0, 0)$, $(0, 0, \frac{1}{2})$
Se	$(\frac{1}{3}, \frac{1}{3}, \pm u)$, $(-\frac{1}{3}, -\frac{1}{3}, \frac{1}{2} \pm u)$, where $u = 0.134$
Muffin-tin radii	
Nb	$0.36a = 1.242$ Å
Se	$0.36a = 1.242$ Å
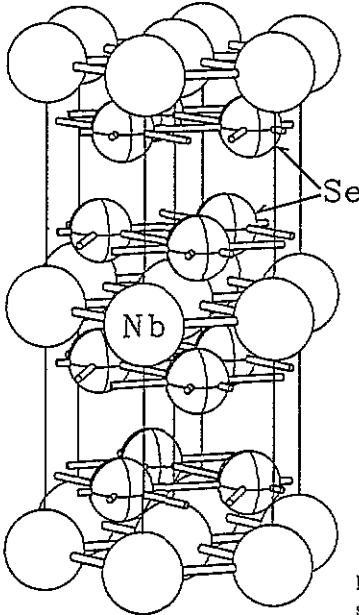
Figure 5. Crystal structure of 2H-NbSe$_2$. Large and small spheres indicate Nb and Se atoms, respectively.

are listed in table 1. We used the crystal structure for the non-CDW state in order to keep the requirements for computer time within reasonable limits.

In the self-consistent calculation, we considered the ^{18}Ar$+3$d$^{10}4$s^2 states for Nb and the ^{18}Ar $+ 3$d^{10} states for Se as 'core' electrons but treated the 4p^6 states for Nb as 'valence' (or band) electrons through use of a second energy window. We found that the core electron charge outside the muffin-tin spheres is very small (0.05% for Nb and 0.02% for Se). The core electrons and the valence electrons were treated scalar relativistically (i.e. all important relativistic effects except the spin–orbit coupling were included) [28] for the spherical component of the potential inside the muffin-tin spheres. Nevertheless, the spin–orbit coupling effect was included in a perturbative way by a second-variational procedure [29]. Inside the muffin-tin spheres, the wavefunctions, charge densities and potential were expanded in terms of spherical harmonics. The cut-off angular momentum (L_{max}) is 7 for the wavefunctions, and 4 for charge densities and potential. The number of augmented plane waves (PWS) is determined by the K_{max} (largest wavevector). We used $K_{max} = 2.85$ equivalent to about 350 PWS. The new charge densities were obtained from the calculated FLAPW wavefunctions at 21 k-points in the $\frac{1}{24}$ irreducible Brillouin zone (IBZ).

After the self-consistent calculation, the density of states was obtained from the energy
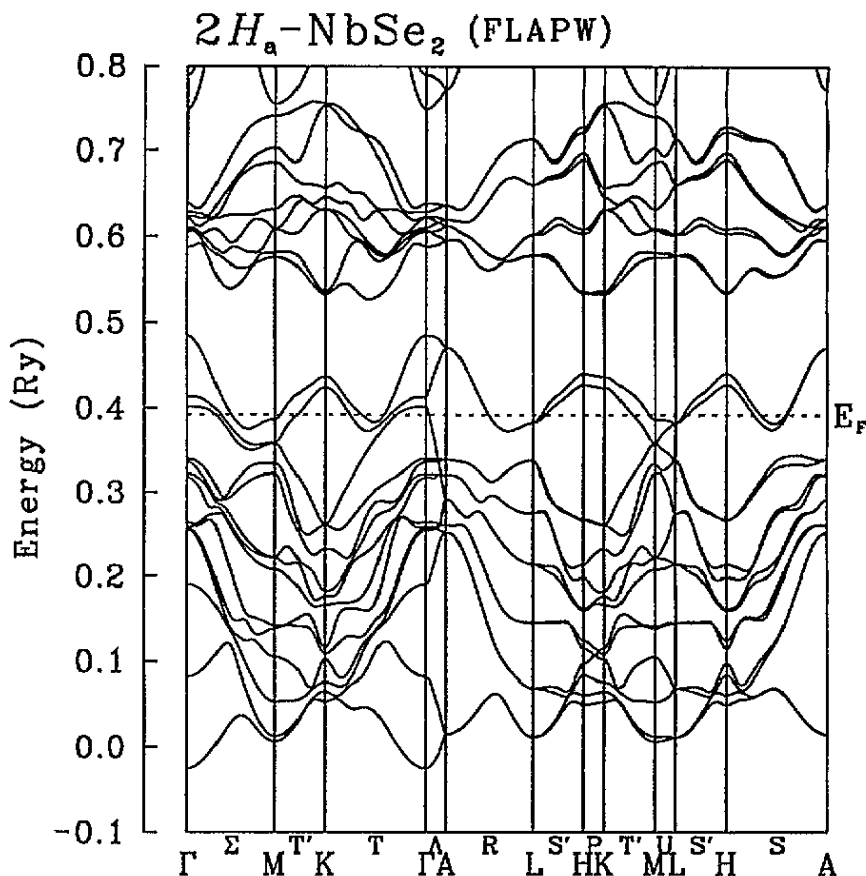
Figure 6. FLAPW band structure of 2H-NbSe₂. The dashed line indicates the Fermi level (0.3925 Ryd). Se 4s bands located between −0.6 Ryd and −0.5 Ryd are not shown. Note that the spin–orbit interactions lift the degeneracy at the K point and on the A–L–H plane except the A–R–L axes.

bands generated on a fine mesh of 305 k-points in the $\frac{1}{24}$ IBZ. The density of states, the Fermi surface and its extremal cross-sectional areas were obtained using the method of Harima *et al* [30]. The calculated band structure and the density of states for 2H-NbSe₂ are shown in figures 6 and 7, respectively. The Fermi level is 0.3925 Ryd and the density of states at the Fermi level is 38.7 states Ryd^{-1}/Nb. The linear specific heat coefficient, γ, is calculated to be 6.7 mJ mol^{-1} K^{-2}. In figure 6, the lowest 12 bands are chalcogen p bands and the 10 bands between 0.37 Ryd and 0.75 Ryd are metal d bands. The Fermi level is seen to intersect three bands from the 16th to the 18th. The 16th band produces a small flat ellipsoidal Fermi surface around the Γ point as shown figure 8(a). Two cylindrical Fermi surfaces are derived from both the 17th and 18th bands, as shown in figure 8(b), (c). Finally, figure 9 shows the angular dependence of the calculated cross-sectional areas of the Fermi surface. The cyclotron masses have also been calculated and are given in table 2.

In the band structure, the origin of the two low-lying d bands separated from the others has already been discussed [19]. Here we analyse the Se p dominant bands. As shown in figure 5, 2H-NbSe₂ has a layered crystal structure with each basal plane having a triangular lattice. Consequently, the Se p_x and p_y dominant bands are almost frustrated along the Λ-axis in the BZ. In contrast, Se p_z bands have large dispersions along the Λ-axis, reflecting
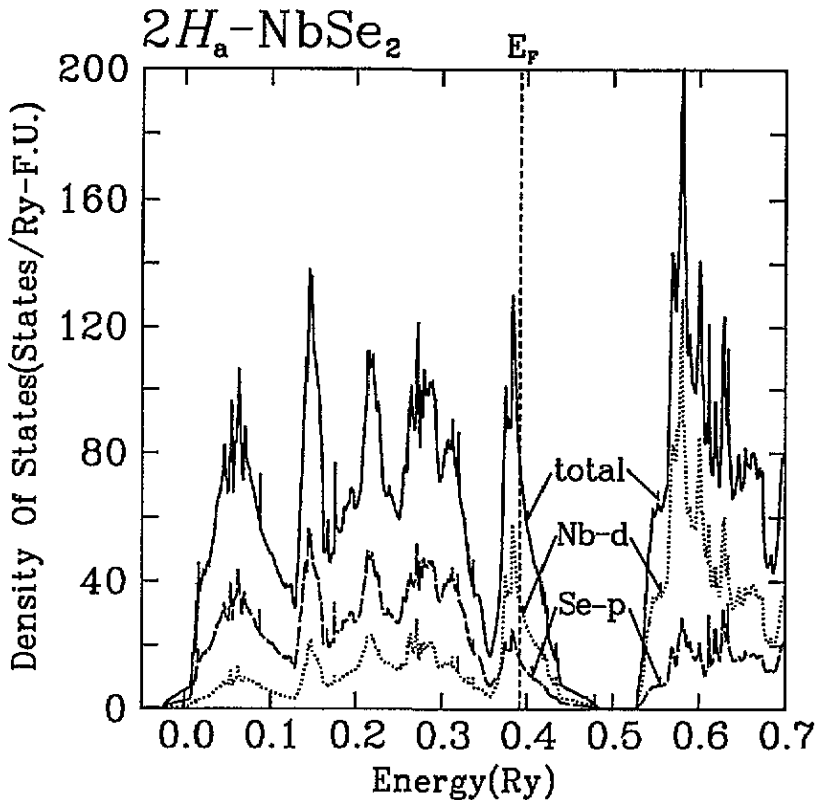
Figure 7. Calculated density of states for 2H-NbSe$_2$ (in units of states Ryd^{-1} FU^{-1}). Solid, dotted and dashed lines show total density of states, Nb d component and Se p component, respectively. The vertical dashed line denotes the Fermi level (0.3925 Ryd). Note that below 0.37 Ryd the Se p component dominates whilst above 0.37 Ryd the Nb d component dominates.

the large intra-layer (intra Se–Nb–Se sandwich) and inter-layer hybridization. At the A point, the inter-layer interactions exactly cancel, because the states have the opposite phase on the next nearest sandwich. However, along Λ, the p$_z$ states are split into a bonding and an anti-bonding state, due to the inter-layer interactions. It is the inter-layer interactions in the vicinity of the Γ point that produce the shape of the Fermi surface shown in figure 8(a).

In summary, the overall disposition of Nb d and Se p dominant bands is similar to that in the previous calculation [19–21]. However, this self-consistent FLAPW approach yields an additional small closed hole Fermi surface of Se p band character around the Γ point due to the overlap between d and p bands. This is the most important result of the present calculation.

6. Discussion

It is clear that this difference between present and previous calculations is caused by the fact that the previous calculations were not self-consistent and used muffin-tin potentials. The p–d overlap follows the charge transfer from the metal to the chalcogen site which raises the p bands relative to the d bands, making self-consistency important. We have also performed
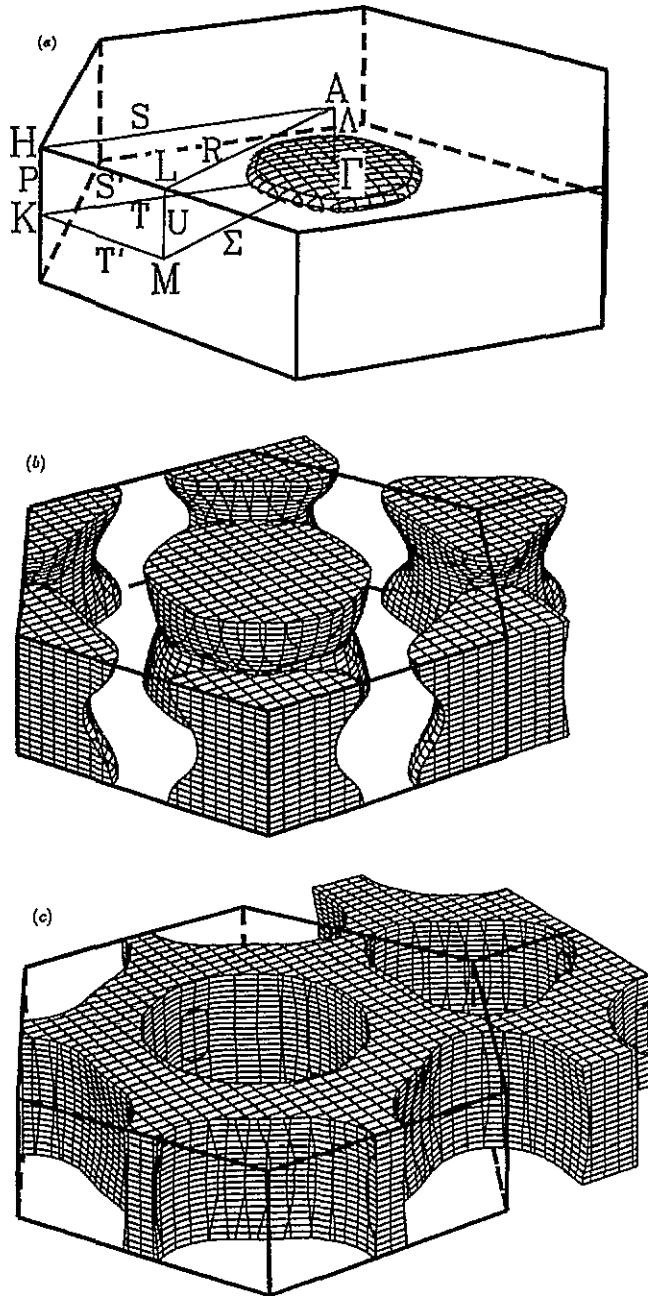
Figure 8. (a) The hole Fermi surface in 2H-NbSe$_2$ around the Γ point derived from the 16th band. (b) The hole Fermi surface derived from the 17th band. (c) The electron Fermi surface derived from the 18th band.

a self-consistent calculation within the muffin-tin approximation, and found that the p–d overlap was much larger and that the Fermi surface differed from the full-potential one. This indicates that the muffin-tin potential approximation overestimates the charge transfer and is rather inaccurate for these open, layered structures. There is strong experimental
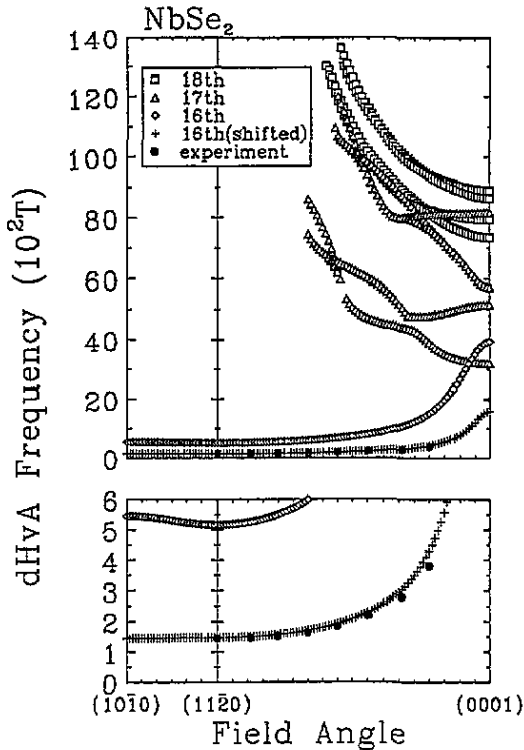
Figure 9. Angular dependence of calculated extremal cross-sectional areas, i.e. DHVA frequencies, of the Fermi surface for the non-CDW state of 2H-NbSe$_2$. In the bottom enlarged diagram, experimental points are shown as solid circles.

evidence of the p–d overlap in the angle resolved x-ray photoemission experiments [31], although they were compared at the time with the earlier band structure calculation [20]. We find these photoemission spectra can be re-interpreted in terms of the present band structure with better overall agreement.

While previous calculations [19–21] did not give rise to any Fermi surface sheets that could be responsible for the measured DHVA oscillations, the angular dependence of the DHVA frequency predicted here qualitatively agrees with experiment. Although the calculated frequency for this small hole pocket around the Γ point is three times too large, an upwards shift of the Fermi level by 7 mRyd brings the calculated and measured frequencies into good agreement as shown in figure 9. The remaining discrepancy may be attributed to the local density approximation which is known to give smaller band gaps in semiconductors and, in the case of layered transition metal dichalcogenides, to overestimate the p–d band overlap [32].

Cylindrical Fermi surfaces derived from 17th and 18th bands and shown in figures 8(b) and (c) are very similar to those of the isostructural compound, 2H-TaSe$_2$. The DHVA oscillations in the commensurate CDW phase of 2H-TaSe$_2$ were explained in terms of the calculated non-CDW band structure by assuming band folding [33]. However, in 2H-NbSe$_2$, DHVA frequencies relating to the cylindrical surfaces have not yet been detected, even in the normal state. On the other hand, the recent experiments using the two-dimensional angular correlation of positron annihilation radiation [34] does appear to reveal the cylindrical

Table 2. Calculated and measured DHVA frequencies and cyclotron masses. In parentheses, the values with the Fermi energy shifted upward by 7 mRyd are also shown for the 16th band.

	Calculation		Experiment	
Field direction	Frequency (T)	Cyclotron mass (m_0)	Frequency (T)	Cyclotron mass (m_0)
16th band				
$(10\bar{1}0)$	546.1(144.6)	0.48(0.47)		
$(11\bar{2}0)$	518.2(148.1)	0.43(0.48)	144	
$20°$ to $(11\bar{2}0)$	551.3(157.4)	0.46(0.52)	152	0.61
(0001)	3934.6(1587.7)	2.27(4.09)		
17th band				
(0001)	8172.0	1.60		
(0001)	5732.3	2.15		
(0001)	5168.2	2.04		
(0001)	3204.6	1.32		
18th band				
(0001)	8873.1	1.98		
(0001)	8637.6	1 92		
(0001)	7946.3	2.61		
(0001)	7352.8	2.24		

topology. We believe that experimental limitations relating to crystals of inadequate quality are chiefly responsible for us not detecting quantum oscillations originating from these larger cylindrical Fermi surface sheets in the present work. Finally, the incommensurate CDW q-vector may also cause difficulty in the detection of quantum oscillations. This effect may be unimportant on the small Γ-centred surface, but may be significant for the larger structures.

Having established a credible electronic structure, we now wish to comment on the mass-enhancement factor in 2H-NbSe$_2$. The measured cyclotron mass at $70°$ from the c-axis $m_{\text{expt}} = 0.61m_e$, when compared to the calculated band-mass value of $m_{\text{cal}} = 0.46m_e$, indicates a mass-enhancement factor, $\lambda_{e-ph} = 0.3$, for the Se p dominant bands ($m_{\text{expt}}/m_{\text{cal}} = 1 + \lambda_{e-ph}$). On the other hand the measured specific heat coefficient, $\gamma = 18.5$ mJ mol^{-1} K^{-2} [35], when compared to the calculated value of 6.7 mJ mol^{-1} K^{-2}, suggests an overall mass-enhancement factor, $\lambda_{e-ph} = 1.8$. This discrepancy is probably due to the contributoins to γ predominantly arising from electrons in bands 17 and 18 rather than the small band 16 ellipsoid. However, the effective masses for the 17th and 18th bands would have to be measrued to prove this. We also note that the effects of the CDW were not included in the present calculation, and that a previous band structure calculation [36] showed that the density of states at the Fermi level would be reduced in the presence of the CDW. The overall mass-enhancement factor of 1.8 may therefore be an underestimate, even though calculated values considerably less than this (0.89) are reported [35].

Moreover, isostructural 2H-NbS$_2$, which is also a superconductor but does not form a CDW state, also has a large γ-value (17.64 mJ mol^{-1} K^{-2} [35], 19.3 mJ mol^{-1} K^{-2} [37]) and a relatively high T_C (6.1 K [38]) whereas both 2H-TaSe$_2$ and 2H-TaS$_2$, which are expected to have similar electronic structures, have smaller γ-values, and lower values of T_C (8.6 mJ mol^{-1} K^{-2} [39], 0.2 K and 0.8 K respectively [40]), and both have CDW instabilities. Large mass-enhancement factors for 2H-Nb dichalcogenides are evidently consistent with high values of T_C. Finally, we note that with $\lambda_{e-ph} = 1.8$ in 2H-NbSe$_2$,

then, from the calculated c-axis cyclotron masses in table 2 for the cylindrical Fermi surface, $m_{cal} = 1.3m_e$ and $2.6m_e$, we anticipate measured values $(= (1 + \lambda_{e-ph})m_{cal})$ of $3.6m_e$ and $7.3m_e$. These relatively large masses when combined with expected damping due to impurity scattering occurring in these higher-frequency orbits, would account for the absence of quantum oscillations arising from these large sheets of Fermi surface in the present experiment.

7. Conclusions

Our detailed experimental and theoretical scrutiny of quantum oscillations in 2H-NbSe$_2$ leads to a consistent picture of these effects in the normal state. In a new self-consistent FLAPW calculation we have identified a hole pocket about the Γ point which could be responsible for the observed DHVA frequency and have presented plausible arguments for not seeing the other Fermi surface pieces predicted by our calculations.

As for the persistence of the DHVA oscillations into the superconducting state we have extended the measurements to fields of $\sim 0.3B_{C2}$ and to temperatures of $\sim 0.003T_C$. The new data are consistent with previous measurements and with the interpretation that, as with other type II superconductors, the oscillations are due to the intrinsic gaplessness of the mixed state. However, the nature of the quasi-particle orbits which give rise to the oscillations of the magnetization has not been determined. To be precise we have observed a small field-dependent damping, as predicted by the theories in [12] and [13], but not of the magnitude expected from the gap value of 1.1 meV, as measured in infra-red and Raman scattering experiments [25, 26]. Nevertheless we note that, at least near B_{C2}, the data are compatible with the theory for a zero-field gap of 0.6 meV.

Evidently, observation of the predicted cylindrical Fermi surface sheets would help to clarify the situation. If such measurements were consistent with larger gaps and a mass-enhancement factor $\lambda = 1.8$ then the small gap (0.6 meV) and small λ (0.3) on the Γ-centred ellipsoidal pocket could be attributed to the much weaker electron–phonon coupling on this Se p-state-related feature of the Fermi surface than on the other sheets formed by the Nb d bands. Finally we suggest that in the light of this plausible scenario, it is premature to speculate on the existence of exotic pairing in NbSe$_2$.

Acknowledgments

References

[1] Graebner J E and Robbins M 1976 *Phys. Rev. Lett.* **36** 422
[2] Onuki Y, Umehara I, Ebihara N, Nagai N and Takita K 1992 *J. Phys. Soc. Japan* **61** 692
     Onuki Y, Umehara I, Ebihara T, Albessard A K, Satoh K, Takita K, Aoki H, Uji S and Shimuzu T 1993 *Physica* B **186–188** 1050
[3] Fowler C M, Freeman B L, Hults W L, King J C, Mueller F M and Smith J L 1992 *Phys. Rev. Lett.* **68** 534
[4] Kido G, Komorita K, Katayama-Yoshida H and Takahoshi T 1991 *J. Phys. Chem. Solids* **52** 1465

[5]   Haanappel E G, Joss W, Wyder P, Askenazy S, Mueller F M, Trübenbach K, Mattausch H J, Simon A and Osofsky M 1993 *J. Phys. Chem. Solids* **54** 1261

[6]   Haanappel E G, Joss W, Vagner I D, Wyder P, Trübenbach K, Mattausch H J, Simon A, Mueller F M and Askenazy S 1993 *Physica* C **209** 39

[7]   Mueller F M, Lowndes D H, Chang Y K, Arko A J and List R S 1992 *Phys. Rev. Lett.* **68** 3928

[8]   Corcoran R, Harrison N, Hayden S M, Meeson P, Springford M and van der Wel P J 1994 *Phys. Rev. Lett.* **72** 701

[9]   Harrison N, Hayden S M, Meeson P, Springford M, van der Wel P J and Menovsky A 1994 to be published

[10] Goodrich R G *et al* 1993 *J. Phys. Chem. Solids* **54** 1251

[11] Van der Wel P J, Caulfield J, Hayden S M, Meeson P, Singleton J and Springford M 1994 to be published

[12] Maki K 1991 *Phys. Rev.* B **44** 2861

[13] Wasserman A and Springford M 1994 *Physica* B **194–196** 1801

[14] Markiewicz R S, Vagner I D, Wyder P and Maniv T 1988 *Solid State Commun.* **67** 43

[15] Miyake K 1993 *Physica* B **186–188** 115

[16] Stephen M J 1991 *Phys. Rev.* B **43** 1212

[17] Maniv T, Rom A I, Vagner I D and Wyder P 1992 *Phys. Rev.* B **46** 8360

[18] Norman M 1990 *Phys. Rev.* B **42** 6762

[19] Mattheiss L F 1973 *Phys. Rev.* B **8** 3719

[20] Wexler F G and Woolley A 1976 *J. Phys. C: Solid State Phys.* **9** 1185

[21] Fong C Y and Cohen M L 1974 *Phys. Rev. Lett.* **32** 720

[22] Brandt U, Pesch W and Tewordt L 1967 *Z. Phys.* **201** 209

[23] Berthier C, Molinie P and Jerome D 1976 *Solid State Commun.* **18** 1393

[24] Shoenberg D 1984 *Magnetic Oscillations in Metals* (Cambridge: Cambridge University Press)

[25] Clayman B P and Frindt R F 1971 *Solid State Commun.* **9** 1881

[26] Lee D H, Dubeck L W and F Rothwarf 1975 *Phys. Lett.* **53** 379

[27] Gunnarson O and Lundqvist B I 1976 *Phys. Rev.* B **13** 4274

[28] Koelling D D and Harmon B N 1977 *J. Phys. C: Solid State Phys.* **10** 3107

[29] Takeda T and Kubler J 1979 *J. Phys. F: Met. Phys.* **9** 661

[30] Harima H, Yanase A and Hasegawa A 1990 *J. Phys. Soc. Japan* **59** 4054

[31] Minami F, Sekita M, Aono M and Tsuda N 1979 *Solid State Commun.* **29** 459; 1979 *Solid State Commun.* **30** 731

[32] Benesh G A, Woolley A M and Umrigar C 1985 *J. Phys. C: Solid State Phys.* **18** 1595

[33] Wilson J A 1977 *Phys. Rev.* B **15** 5748

[34] Takita K, Umehara I, Ebihara T, Nagai N, Nakashima H, Kubota T, Kondo H, Onuki Y and Tanigawa S 1991 *Physica* C **185–189** 2717

[35] Garoche P, Veyssie J J, Manuel P and Molinie P 1976 *Solid State Commun.* **19** 455

[36] Doran N J and Woolley A M 1981 *J. Phys. C: Solid State Phys.* **14** 4257

[37] Hamaue Y and Aoki R 1986 *J. Phys. Soc. Japan* **55** 1327

[38] Dahm D C, Carolan J F and Haering R R 1986 *Phys. Rev.* B **33** 5214

[39] Garoche P, Manuel P, Veyssie J J and Molinie P 1978 *J. Low. Temp. Phys.* **30** 323

[40] Wilson J A, DiSalvo F J and Mahajan S 1975 *Adv. Phys.* **24** 117